Assessing the Protonation State of Drug Molecules: The Case of Aztreonam

Natalia Díaz,[†] Tomás L. Sordo,[†] Dimas Suárez,*[,†] Rosa Méndez,[‡] Javier Martín Villacorta,[‡] Luis Simón,[§] Manuel Rico,[§] and M. Ángeles Jiménez[§]

Departamento de Química Física y Analítica, Universidad de Oviedo, Julián Clavería 8, 33006 Oviedo (Asturias), Spain, Departamento de Química, Física y Expresión Gráfica, Universidad de León, 24071 León, Spain, and Instituto de Química-Física Rocasolano, Consejo Superior de Investigaciones Científicas, Serrano 119, 28006 Madrid, Spain

Herein we examine the viability of physicochemical approaches based on standard computational chemistry tools to characterize the structure and energetics of flexible drug molecules with various titratable sites. We focus on the case of the monobactam antibiotic aztreonam, whose structure and physicochemical properties have been ascribed to several tautomeric forms, although it is still unclear which protonation states are responsible for its biological activity. First, we experimentally determined the pK_a values for aztreonam over the pH range 0.8−7.0 using both ^{1}H NMR and ^{13}C NMR spectroscopy. Second, we carried out quantum chemical calculations on snapshots extracted from classical molecular dynamics simulations. Various levels of approximation were used in the energy calculations: ONIOM(HF/3-21G*:AMBER) for geometry relaxation, B3LYP/6-31+G** for electronic and electrostatic solvation energies, and molecular mechanics for attractive dispersion energy. The value of the free energy of solvation of a proton was treated as a parameter and chosen to give the best match between calculated and experimental pK_a values for small molecules. Overall, this computational scheme can give satisfactory results in the pK_a calculations for drug molecules.

Introduction

Electrostatic interactions are key factors in determining the properties of drug molecules including their pharmacological functions, such as ligand binding, absorption, and transport as well as their structure and resistance to chemical and enzymatic degradation. The electrostatic properties of a molecule can dramatically change depending on the protonation states of its titratable groups, which, in turn, depend on their intrinsic chemical properties, substituent effects, ionization state of other titratable sites, and the pH and ionic strength of the surrounding solvent. Consequently, pK_a is one of the main physicochemical properties afecting the drug likeness of a molecule.[1] For example, the bioavailability of compounds has been proposed to be governed by several properties depending on the predominant protonation state at biological pH.[2] However, most often, the pK_a values or the protonation state responsible for activity or both have not been reported for molecules of therapeutic importance.[3] Moreover, many different ionization states for a compound are often neglected in rational drug design because of the lack of robust protocols for routine estimation of pK_a values.[4]

Aztreonam (AZR) was the first marketed monobactam antibiotic.[5] It is specifically active against aerobic gram-negative bacteria and exhibits a high degree of stability to β-lactamases. Scheme 1 shows some tautomeric forms of AZR differing in the protonation state of the thiazol ring, the carboxyl group, and the amino group, which are all located in the 4-acylamino side chain attached to the β-lactam nucleus. The chemical structures sketched in Scheme 1 correspond to zwitterionic (**Z1**, **Z2,** and **Z3**), anionic (**A1**−**A4**), or dianionic (**D1**) forms.

On the basis of a survey of the scientific literature and/or chemical databases, it is unclear as to which AZR protonation states is biologically active. For example, earlier articles usually depict AZR in its **Z2** configuration;[5,6] the AZR entry in the Pubchem database[7] also corresponds to the **Z2** zwitterionic form; the ZINC database[8] generates an (unlikely) anionic tautomer with a protonated *N*-SO_3H moiety; and the CAS electronic record of AZR (78110-38-0) displays a fully neutralized tautomer. However, the crystal structure of AZR (cocrystallized with dimethylacetamide) has been shown to unambiguously correspond to the **Z1** structure.[9] In the crystallographic study on the *C. freundii* acyl-enzyme,[10] AZR was initially modeled as a monoanion in the **A1** form. However, the apparent pK_a values of AZR were indirectly determined by solubility measurements,[6] the reported pK_a values for the sulfonyl, amine, and carboxyl groups being −0.7, 2.75, and 3.91, respectively. Similar pK_a values are predicted by the SPARC method,[11] which combines an empirical fragment-type approach with a linear free energy treatment. However, the SPARC online calculator[12] assigns the highest pK_a value (4.34) to the *N*-thiazol atom followed by the pK_a value for the carboxyl group (2.70). Regardless of the precise assignment of the pK_a values, these pK_a calculations indicate that AZR should exist as a dianion (**D1**) in aqueous solution at physiological pH. In consonance with this, two negative charges are assumed for AZR in the experimental studies on the diffusion of β-lactams through liposome membranes.[13,14]

As described above, the structure and physicochemical properties of AZR have been ascribed to (at least) four different protonation states (**Z1**, **Z2**, **A1**, **D1**) and there are significant doubts about the assignment of the pK_a values. We lack information about the actual free energy differences among these and other protonation states of AZR as well as their structural and dynamical properties. The acquisition of this knowledge could be useful in shedding light onto some characteristics of AZR activity such as its resistance against the broad-spectrum metallo-β-lactamases.[15] Intriguingly, the active site of these enzymes can accommodate β-lactam substrates with very different side chains attached to the β-lactam core. Whether AZR cannot bind to the metallo-β-lactamases or binds but in a

* Corresponding author. Phone: +34 985 18 22 66. Fax: +34 985 10 31 25. E-mail: dimas@uniovi.es.
[†] Universidad de Oviedo.
[‡] Universidad de León.
[§] Consejo Superior de Investigaciones Científicas.

10.1021/jm060096t CCC: $33.50
Published on Web 05/06/2006

Scheme 1. Tautomeric Forms of Aztreonam Considered in This Work

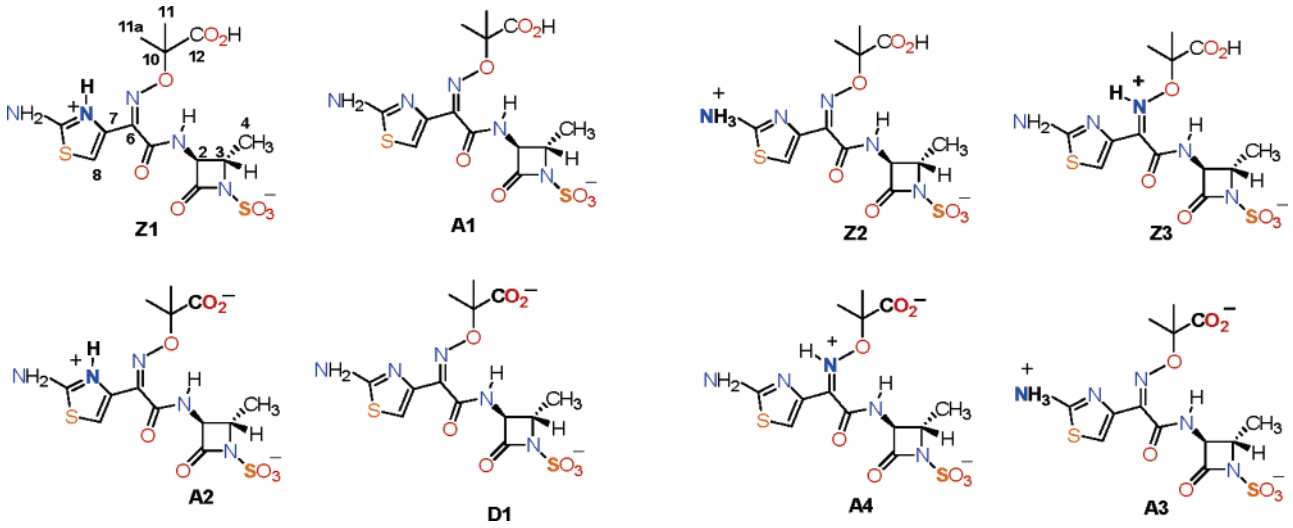

nonproductive orientation must be critically related to its most populated protonation state.

The case of AZR prompted us to consider the viability of physicochemical approaches based on standard computational chemistry tools to predict the relative free energies of different tautomers of drug molecules, thereby improving our knowledge of their biological mode of action and their pharmacokinetic properties. First, we experimentally re-examined the pK_a values for AZR over the pH range 0.8−7.0. The electrostatic behavior of titrating groups in AZR was investigated by using both ^{1}H NMR and ^{13}C NMR spectroscopy. Nonlinear least-squares fits of simple relationships derived from the Henderson−Hasselbalch equation to the chemical shifts versus pH data led to the unambiguous determination of ionization constants. Second, we developed and tested a novel computational scheme, which combines classical molecular-dynamics (MD) and quantum-mechanical (QM) calculations, resulting in a mixed continuum/discrete representation of the solute−solvent interactions. This MD/QM approach represents an extension of previous theoretical work that has demonstrated that the combination of QM methods with continuum dielectric solvation models can provide quantitatively good pK_a predictions (less than ±1 pK_a unit) for small closely related solutes. [16−26] Moreover, computational strategies based on ab initio QM calculations are beginning to be used for the prediction and rationalization of pK_a values of ionizable residues in proteins.[27] In our approach, QM calculations are performed for multiple solute conformations extracted from classical MD simulations to determine the pK_a values by carrying out a statistical mechanical average over the conformations. In addition, protonation sampling among the several titratable groups of AZR is taken into account to compute the global pK_a values. The experimentally derived and calculated pK_a values are discussed in light of the biological activity of AZR. Finally, some potential benefits of systematically applying the MD/QM computational approach to drug molecules are discussed.

Results

pH Dependence of ^{1}H and ^{13}C Chemical Shifts. To experimentally determine pK_a values in the AZR molecule as well as to assess the functional group or groups responsible for them, changes in the^{1}H chemical shifts were measured as a function of pH in an aqueous solution at 25 °C, and the pH variation of ^{13}C chemical shifts was followed in a D_2O solution. pH values ranged from 0.85 to 7.0. The β-lactam ring of AZR irreversibly opened at pH values of more than 7.0. Those protons and carbons displaying chemical shift changes less than 0.01 and 0.2 ppm, respectively, over the whole pH range studied were considered to be pH independent. They correspond to protons H-2, H-3, and H-4 and to carbons C-2, C-3, and C-4, which are located at the β-lactam moiety of the AZR molecule (see C atom numbering in Scheme 1). This result is the expected one, taking into account the fact that the pK_a value for the sulfonate group attached to the β-lactam moiety is below pH 0.85.

Chemical shifts corresponding to protons amide NH, H-8, H-11, and H-11a and to carbons C-6, C-7, C-8, C-11, and C-12 are strongly pH dependent (Figure 1 and Figure S2 in Supporting Information). The observed total chemical shift changes are, in absolute value, 0.12−0.22 ppm for the protons and 1.1−10.9 ppm for the carbons. To derive pK_a values, titration curves for protons and carbons were independently analyzed because they were obtained from AZR samples in H_2O/D_2O 9:1 v/v and in pure D_2O, respectively. Assuming a single pK_a value, nonlinear fits of the corresponding Henderson−Hasselbach equation to either the proton or the carbon titration curves were very poor, showing large deviations from the experimental data points. Therefore, a nonlinear regression procedure to eq 1, which is derived from Henderson−Hasselbach equation for a noninteracting model and assumes two different pK_a values and rapid equilibrium between protonated and deprotonated forms,[28,29] was fit to the titration data

$$\delta = \frac{\delta_{AH2}10^{(pK_{a1} + pK_{a2} - 2pH)} + \delta_{AH}10^{(pK_{a1} - pH)} + \delta_A}{10^{(pK_{a1} + pK_{a2} - 2pH)} + 10^{(pK_{a1} - pH)} + 1} \quad (1)$$

where δ_A, δ_{AH}, and δ_{AH2} represent individual chemical shift values of the observed resonance in the different protonation states. Least-squares analysis was performed by assuming identical pK_{a1} and pK_{a2} for all considered protons and for all considered carbons. The ^{1}H and ^{13}C chemical shifts corresponding to each of the three AZR protonated forms obtained from the fittings are listed in Table 1. There is a good agreement between the values derived from ^{1}H chemical shifts (pK_{a1} = 2.70, pK_{a2} = 4.19) and from ^{13}C chemical shifts (pK_{a1} = 2.49, pK_{a2} = 4.34). Although it is commonly assumed that pK_a values determined in D_2O and expressed in pH* units (uncorrected

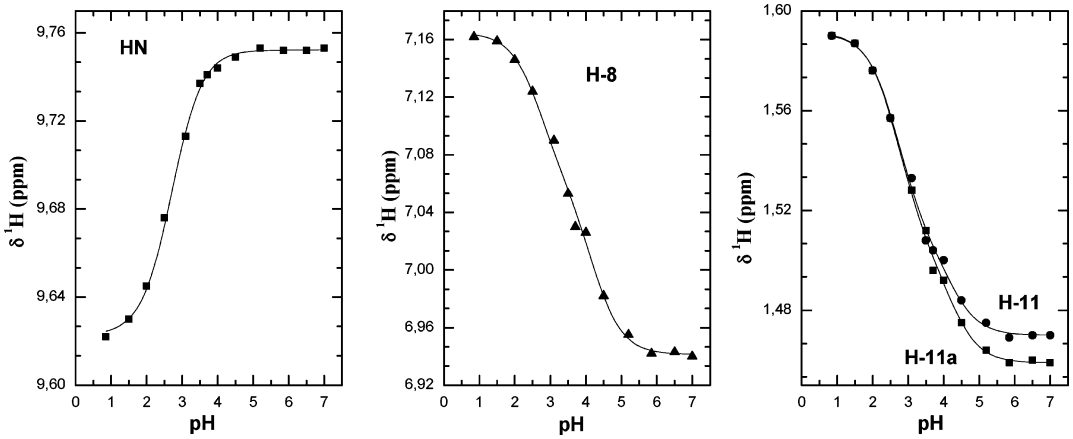

Figure 1. Titration curves for protons for amide NH (left), H-8 (center), and methyl groups H-11 and H-11a (right). Symbols correspond to the observed ^{1}H δ-values. The fit of eq 1 is shown as a continuous line.

Table 1. ^{1}H and ^{13}C Chemical Shifts Values for the Three AZR Protonated Forms Considered for pK_a Determination that Are Obtained by Fitting to Eq 1[a]

	δ_{AH2}	δ_{AH}	δ_A
		^{1}H	
amide NH	9.623 ± 0.002	9.749 ± 0.003	9.752 ± 0.002
H-8	7.165 ± 0.002	7.061 ± 0.006	6.941 ± 0.002
methyl H-11	1.591 ± 0.002	1.509 ± 0.003	1.470 ± 0.002
methyl H-11a	1.591 ± 0.002	1.506 ± 0.004	1.459 ± 0.002
		^{13}C	
C-6	145.7 ± 0.08	146.6 ± 0.10	150.3 ± 0.06
C-7	132.6 ± 0.09	136.1 ± 0.18	143.5 ± 0.07
C-8	114.3 ± 0.08	114.3 ± 0.09	115.5 ± 0.06
C-11	25.6 ± 0.08	26.3 ± 0.09	26.7 ± 0.06
C-12	180.0 ± 0.09	182.4 ± 0.12	184.7 ± 0.06

[a]Reported errors are the standard fitting errors.

pH) are similar to the corresponding values determined in H_2O and expressed in pH units,[30] the slight differences between the two sets of values arise most probably from isotopic effects.

To experimentally assess which of the two possible acidic groups, *N*-thiazol or carboxylic acid, corresponds to each deprotonation step, we examined the magnitudes of the chemical shift changes in all pH dependent protons and carbons. Ideally, some protons and carbons would report only one of the pK_a values, and this pK_a value will correspond to their closest titrating group. This strictly occurs only for one proton and one carbon: (a) the NH amide proton that has identical δ_{AH} and δ_A (within error range; Table 1) values and (b) the C-8 carbon with identical δ_{AH2} and δ_{AH} (within error range; Table 1) values. Thus, the NH amide proton that is closer to the carboxylate group than to the *N*-thiazol senses only pK_{a1}, and the C-8 carbon that is on the thiazol ring sees only pK_{a2}. All of the other pH dependent protons and carbons are sensitive to both deprotonations. The fact that in general the change in chemical shift for those protons and carbons closer to the *N*-thiazol group is larger between pH values 3.5 and 7.0 than between 0.85 and 3.5 (Figure 2) while the variation for those protons and carbons closer the carboxylate group is smaller between pH values 3.5 and 7.0 than between 0.85 and 3.5 (Figure 2) provides further support that pK_{a1} and pK_{a2} correspond to the carboxylate and *N*-thiazol groups, respectively.

MD Simulations. To understand the conformational properties of AZR, we carried out 3 ns MD simulations of the eight AZR tautomers computationally examined in this work (Scheme 1). The systems were fully solvated by a box of water molecules and classically described using our AMBER-like force field for AZR and the popular TIP3P potential for water molecules.

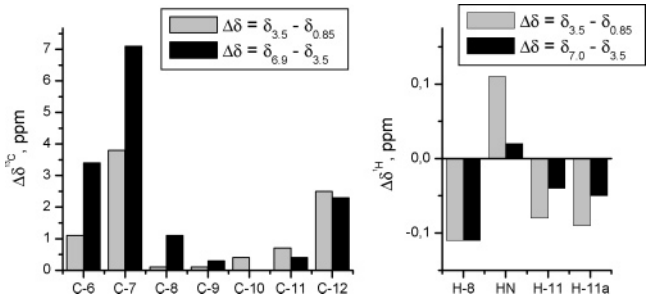

Figure 2. Change in chemical shift for pH dependent protons (right) and carbons (left).

The eight AZR isomers corresponded to three zwitterionic structures (**Z1**−**Z3**), four anionic **(A1**−**A4)** structures, and one dianionic structure (**D1**). The selection of the AZR protonation states is in agreement with the experimental fact that AZR exists as a zwitterion, anion, and dianion in the pH interval 0−10. The AZR tautomers shown in Scheme 1 differ in the protonation state of their acid−base groups, namely, the carboxyl group, the exo-cyclic amino group, and the *N*-thiazol atom. Note that in this pH interval the *N*-SO_3^- group must be deprotonated owing to its strong acidic character.

The **A3**, **A4**, **Z2**, and **Z3** states of AZR are found to be high energy configurations of AZR (see below). Therefore, we focus here on the structural and dynamical features of the most stable protonation states, namely, **Z1**, **A1**, **A2**, and **D1**. The superposition of their most important cluster representatives is shown in Figure 3. On the basis of their root-mean-square similarity, the representative structures account for ∼80% of the sampled snapshots of each trajectory. Note that the thickness of the individual models is proportional to the population of the corresponding clusters.

According to our simulations, the flexibility of the AZR side chain mainly arises through internal rotations about the C2−N and C10−O bonds. As expected, the protonation state of AZR influences the conformational preferences of its acyl-amino side chain. On the one hand, the AZR side chain shows considerable mobility when the five-membered thiazol ring bears a positive charge (**Z1** and **A2** in Figure 3). The **A2** state exhibits the larger side chain flexibility because in addition to the positive charge on the thiazol N atom, its carboxyl acid is negatively charged. On the other hand, the **A1** and **D1** states, in which the thiazol ring is neutral, adopt a slightly more compact conformation and have lower side chain flexibility as revealed by the clustering analyses. Of particular interest can be the case of the dianionic state **D1**: its side chain is relatively rigid because of an

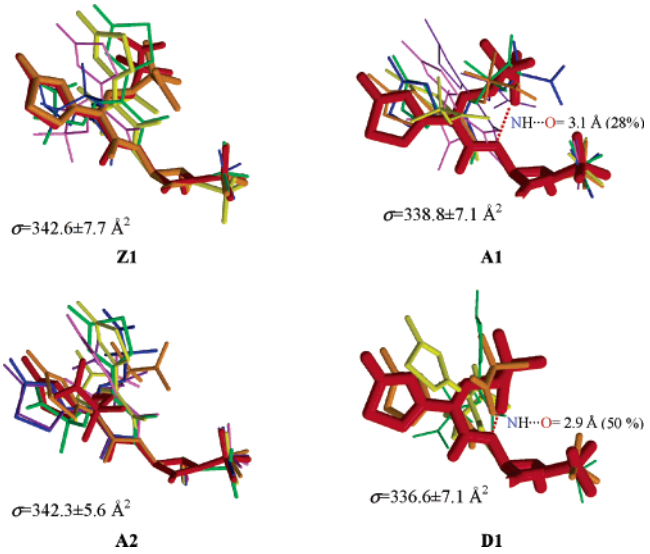

Figure 3. Superposition of the most populated representative structures derived from the clustering analyses of the simulations. The thickness of the models corresponds to the number of snapshots represented by each model. The average values of the molecular surface (σ) as evaluated with molsurf are also indicated.

intramolecular $COO^{-}\cdots H-N$ H-bond that is present in 50% of the analyzed snapshots.

pK_a Calculations. Table 2 contains the relative free energies in solution ($\Delta G_{aq,i}$) of the zwitterionic (**Z1**−**Z3**) and anionic (**A1**−**A4**) forms with respect to the dianionic configuration (**D1**) as a function of pH. The $\Delta G_{aq,i}$ values were obtained using eq 2 with the average values of standard free energies ($\bar{G}^0_{aq,i}$) being computed by means of the combined MD/QM protocol described in the Experimental Section. Figure S4 in the Supporting Information depicts the evolution of standard free energies for the **Z1**, **A1**, **A2**, and **D1** states along the MD trajectories. These plots indicate that the $G^0_{aq,i}$ values remain stable over the 3 ns of snapshot production time. Mean values of $\bar{G}^0_{aq,i}$ were then estimated to within a standard error of only 0.6 kcal/mol.

As mentioned above, the free energy calculations allow us to safely discard the **Z2**, **Z3**, **A3,** and **A4** configurations as likely configurations of the AZR antibiotic in aqueous solution because these states are calculated to be high energy states in the pH interval 0−8. The relative stability of the remaining states, **Z1**, **A1**, **A2**, and **D2**, changes continuously from pH = 0 to 8. Thus, the most stable states at pH 0, 4, and 8 are the zwitterion **Z1**, the anion **A2**, and the dianion **D1** forms, respectively. It must also be noted that the two anionic forms, **A1** and **A2**, are quite close in energy, although **A2** is about 1 kcal/mol more stable.

Table 2 also shows the occupancy of the different states (w_i) as evaluated by a Boltzmann sum for each state. We found that the four configurations are significantly populated at intermediate values of pH (2−4) because the free energy differences among them are not large. Then, we computed the fractional charges (f(HX)) of the thiazol and carboxyl groups simply as the sum of the w_i values for all of the states where the corresponding group is protonated. A plot of f(HX) as a function of pH gave the titration curves of the thiazol and carboxyl groups with a typical sigmoid shape (Figure S5 in Supporting Information). The pK_a value for each group was determined from the calculated titration curves as the pH where the group (thiazol or carboxyl) is half-protonated. The predicted pK_a values for carboxyl and thiazol are 2.55 and 4.45, respectively. These pK_a values have a statistical imprecision of ±0.8 pK_a units.

For the sake of comparison, we recomputed the $\Delta G_{aq,i}$ values at pH 0 using only one structure for each solvated AZR tautomers, which corresponded to the starting point at their MD trajectories. In this case, the relative $\Delta G_{aq,i}$ values with respect to **D1** are −9.34, −4.14. −2.43, 1.74, 1.11, 10.00, and 11.57 kcal/mol for the **Z1**, **A1**, **A2**, **D1**, **Z2**, **Z3**, **A3**, and **A4** states, respectively. Comparing these values with the equivalent ones in Table 2, we see that averaging free energies over representative MD snapshots especially influences the stability of the anionic states **A2**−**A4**. From the one conformation free energy values, the predicted pK_a values for carboxyl and thiazol are 3.50 and 3.33, respectively. These values differ by about 1 pK_a unit from those derived from the average free energies, thus confirming the importance of taking the flexibility of the AZR tautomers in the QM pK_a calculations into account.

^{13}C Chemical Shifts Calculations. As mentioned in the Experimental Section, ab initio NMR calculations of ^{13}C shifts for the **Z1**, **A1**, **A2**, and **D1** configurations were performed with the same relaxed geometries that were employed in the free energy calculations. In this way, we obtained the average ^{13}C chemical shifts for the different C atoms of each AZR configuration. Subsequently, to compute the ^{13}C shifts as a function of pH, the series of δ values of a given C atom corresponding to the **Z1**, **A1**, **A2**, and **D1** configurations were averaged using the Boltzmann factors (w_i) at the pH of interest. The resulting ^{13}C chemical shifts are reported in Table S1 in the Supporting Information section, which shows both experimental and theoretical values at different pH.

A comparison of the calculated Boltzmann weighted ^{13}C δ values with the experiment for selected C atoms (Figure 4) shows that the accuracy of the theoretical values ranges from 1 to 10 ppm depending on the C atom: the more shielded the C atom, the more accurate its theoretical ^{13}C δ. These systematic errors are mainly due to the limitations of the level of theory (incomplete description of correlation energy, basis set effects, etc.). However, for those C atoms adjacent to the acidic N and O atoms (i.e., C7, C8, and C12), the experimentally observed trends in the ^{13}C chemical shifts as functions of pH are reproduced quite well by the NMR calculations. This result is another indication that the **Z1**, **A1**−**A2**, and **D1** configurations are the only populated protonation states of AZR in the pH interval 0−7. For other C atoms less affected by the deprotonation of the *N*-thiazol and carboxyl groups (C2, C4), their theoretical ^{13}C δ values are nearly constant at varying pH, in agreement with experiment (Table S1). There are, however, other C atoms whose ^{13}C chemical shifts are predicted to change upon pH increase (e.g., C1, C10) in contrast to the experimental results. The source of this disagreement between theory and experiment might be related to the limitations of the MD sampling (3 ns of simulation time) and/or solvent effects not taken into account by the PCM model. Nevertheless, we conclude that the overall agreement between computed and experimental ^{13}C δ values is quite good.

Discussion

Protonation State of AZR. Table 3 summarizes both the experimental and theoretical pK_a values of AZR, which were determined in this work as well as the experimental values (pK_{a1} = 2.75, pK_{a2} = 3.91) that have been reported by Florey in his article dedicated to the physicochemical, analytical, and pharmacokinetic properties of aztreonam.[6] Florey's values, assigned to the exo cyclic amine and carboxyl groups, were determined through solubility (S) measurements and by applying the method of Peck and Benet,[31] which uses the X-intercepts in a plot of

Table 2. Relative Free Energies in kcal/mol (ΔG_i) and the Equilibrium Population (w_i) of the AZR States at Different pH Values

	$\Delta G_{aq,i}$					w_i				
i	pH = 0	pH = 2	pH = 4	pH = 6	pH = 7	pH = 0	pH = 2	pH = 4	pH = 6	pH = 7
Z1	−9.58	−4.13	1.33	6.77	9.52	0.997	0.748	0.023	0.000	0.000
A1	−4.78	−2.05	0.68	3.40	4.77	0.000	0.023	0.068	0.003	0.000
A2	−6.16	−3.22	−0.70	2.03	3.39	0.003	0.229	0.695	0.031	0.004
D1	0.00	0.00	0.00	0.00	0.00	0.000	0.001	0.214	0.966	0.996
Z2	2.13	7.58	13.04	18.50	21.23			0.000		
Z3	4.64	10.10	15.56	21.01	23.75			0.000		
A3	7.52	10.26	12.99	15.71	17.08			0.000		
A4	0.16	2.89	5.62	8.34	9.71			0.000		

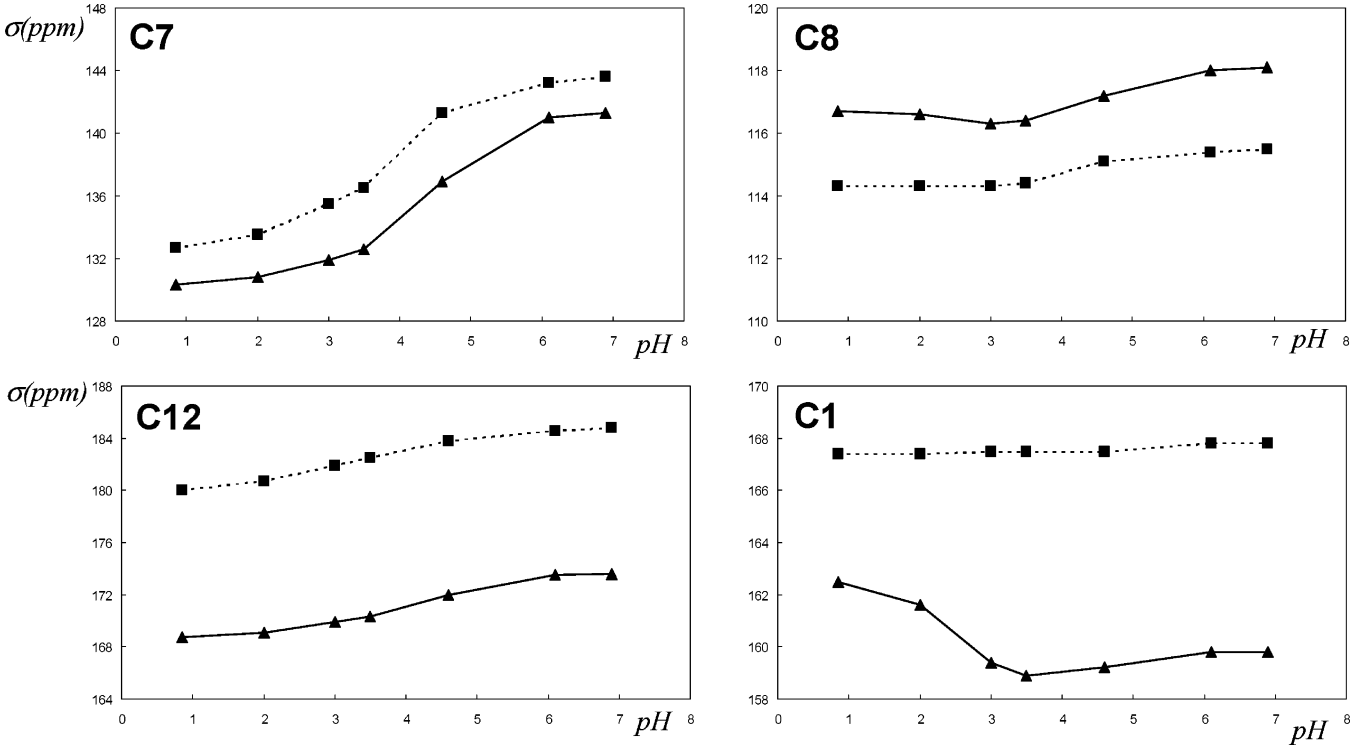

Figure 4. Plots of calculated Boltzmann-weighted ^{13}C δ values (▲, __) and the corresponding experimental values (■, ----) as a function of pH.

Table 3. Summary of the Experimentally/Theoretically Determined pK_a Values for AZR

	from ^1H δ-values (H_2O)[a,b]	from ^{13}C δ-values (D_2O)[a,b]	from MD and QM calc.[a]	from solubility measurements[c]	SPARC empirical values[d]
pK_{a1}	2.70 ± 0.04	2.49 ± 0.08	2.55 ± 0.80	2.75	2.70
pK_{a2}	4.19 ± 0.06	4.34 ± 0.03	4.45 ± 0.80	3.91	4.34

[a] This work. [b] Reported errors correspond to fitting errors. Significant figures for pK_a values do not resemble measurement precision. [c] From ref 6. [d] From ref 11.

$\log(S/S_0 - 1)$ versus pH with S_0 being the lowest solubility measured. In the same article,[6] it is mentioned that the reported pK_a values are in agreement with (unpublished) data obtained by potentiometric, spectrophotometric, and kinetic methods. Table 3 also includes the results of the SPARC web-based calculations of pK_a values. These values were obtained by means of computational automated reasoning in chemistry to estimate chemical reactivity parameters of organic molecules from their fundamental chemical structure. Note that the SPARC method has been parametrized using thousands of physical property data points including 2500 pK_a values in water.

Overall, the agreement among the different pK_a values collected in Table 3 is quite good. For the first ionization constant (pK_{a1}), the differences are only 0.10−0.20 pK_a units, whereas the values for the pK_{a2} constant range from 3.91 to 4.45. Nevertheless, it is reasonable to admit that the newly derived NMR pK_a values supersede the solubility-based pK_a values, thus becoming the best experimental ionization constants of AZR to be compared with the computational values. In this respect, both our MD/QM calculations and the SPARC algorithm predict pK_a values very similar to the experimental ones (differences are less than 0.2 pK_a units). It is also interesting to note how the SPARC values match the NMR experimental results closer than the MD/QM data. This observation was not entirely unexpected given that the SPARC method has achieved considerable success in the prediction of physicochemical properties as shown by an extensive validation by 4550 pK_a values with standard deviation within ±0.25 units for oxy acids and ±0.41 for in-ring N centers.[32]

With regard to the assignment of the AZR pK_a values to specific acid groups, our results coincide with those of the SPARC method in that the lower pK_a (2.50−2.70) belongs unequivocally to the carboxyl group and the higher pK_a (4.1−4.4) to the *N*-thiazol center. We believe that this robust pK_a

assignment corrects the confusing pK_a identification previously reported in the literature (i.e., 2.5 for amine and 3.9 for carboxyl) and clarifies which protonation states of AZR are biologically relevant. Hence, it is now clear that at physiological pH the dianionic structure (**D1)** is the only stable form of AZR. However, as shown by the theoretical calculations, the anionic states **A1** and **A2** are only ~4 kcal/mol above **D1** at pH = 7 so that relatively small environmental changes (electrostatic screening, specific interactions, localization in acidic organelles, etc.) that take place during enzyme−substrate binding or antibiotic diffusion through cell membranes could well stabilize the anionic form of AZR.

The biological relevance of the quasi-energetic **A1** and **A2** anionic states finds support in the crystallographic study of the acyl-enzyme formed between the *C. freundii* β-lactamase enzyme and AZR.[10] We modeled AZR in its **A1** state as suggested by the presence of a direct contact (2.9 Å) observed in the crystal structure between the carboxylic group of the AZR molecule in chain A and the Asp_{123} carboxylate group in chain B. Moreover, according to recent MD calculations,[33] AZR binds to the *C. freundii* β-lactamase active site in its anionic form. (The **D1** state resulted in β-lactamase/AZR interactions unfavorable for catalysis, whereas the anionic **A1** AZR molecule adopted an orientation that was clearly reactive.) Similarly, it may be interesting to note that the stabilization of the **A1** or **A2** states of AZR in an environment with a lower polarity could explain why AZR exhibits a significant rate of diffusion through liposome membranes comparable to those of monoanionic β-lactam antibiotics such as cefoxitin.[13]

MD/QM Calculations. To date, the large majority of the reported QM pK_a calculations have dealt with a series of monoprotic molecules (carboxylic acids, amines, azoles, etc.) for which low energy conformers are readily available. In fact, QM predictions of pK_a values for flexible molecules with various titratable groups are scarce because of the large computational cost that is necessary to generate an ensemble of QM structures. In principle, MD simulations carried out with a hybrid QM/MM Hamiltonian in which the solute molecule is treated quantum mechanically while the water molecules are represented by a classical force field could provide the required structures to perform QM calculations of either energies or molecular properties of solute molecules. Particularly, the use of the SCC-DFTB procedure as the QM method seems very promising because of its computational efficiency.[34] Nevertheless, the computational cost of the QM/MM/MD simulations is still rather high and, consequently, some studies in which purely MM/MD simulations are used to generate the statistical ensemble of solute structures followed by QM calculations of molecular properties have been recently reported.[35,36] It must be noted that this approach can be considered as the QM counterpart of other computational methods, such as the so-called MM-PB method,[37] which predict mean values of the free energies of interaction between biomolecules in solution as estimated over a series of representative snapshots extracted from classical MD simulations.

Our results confirm that carrying out QM calculations on MD snapshots constitutes a straightforward and physically based approach that can give satisfactory results in the pK_a calculations for drug molecules such as AZR, provided that the energy calculations account for all aspects of the proton-binding phenomenon, except for the value of $\Delta G_{solv}(H^+)$, which was considered to be the parameter that gives the best match between calculated and experimental pK_a values for small and relevant molecules. Various levels of approximation can be used in the energy calculations. For example, the internal geometry of solute molecules can be quantum mechanically relaxed at a low level of theory, ensuring that the conformational orientation of the solute is preserved. A standard level of theory (e.g. B3LYP/6-31+G**) combined with an implicit solvent model can take into account both the intramolecular electronic effects and the solute−solvent electrostatic interactions. For some anions, particularly those concentrating charge on a single exposed heteroatom, it has been shown very recently that strengthening implicit solvent calculations with a single explicit water molecule could be adequate to better account for strong short-range hydrogen-bonding interactions between the anion and the solvent.[26] However, other interactions such as attractive dispersion interactions can be accurately empirically calculated. In terms of performance and predictive ability, there is certainly room for further improvement in these and other details of the computational protocol (e.g., using scaling factors on the electronic energies for including thermal contributions). We believe, however, that the extensive sampling performed by the classical MD simulations with an explicit solvent should not be replaced by conformational searching algorithms because the latter may underestimate the contributions of the relatively high energy conformers accessible to the solute molecules.

Because the empirical fragment-based SPARC method predicts accurate pK_a values for AZR, one may question whether MD/QM computational approaches are really needed. One obvious answer is that the MD/QM pK_a calculations have broader applicability because they can take into account the effect of nonaqueous solvents or investigate chemical compounds that are outside commercial databases or training sets. In addition to this, we point out that the set of MD-generated structures complemented with their QM charge densities contains much valuable information for computing QM descriptors of drug-like molecules which, in turn, could be used in the design of more sophisticated physicochemical potentials (scoring functions) to be employed in structure-based drug discovery.[38] With the advent of faster QM methodologies and the decreasing cost of computer hardware, MD and QM calculations could be used soon to enrich databases of drug-like molecules[8] by assessing the free energy of the biologically relevant protonation states and annotating molecules with electrostatic properties and QM descriptors.

Experimental Section

NMR Spectroscopy. NMR spectra were acquired at 25 °C on a 600 MHz Bruker Avance spectrometer equipped with a cryoprobe. The pH values were measured at 22 °C using a Radiometer pH meter calibrated with standard solutions at pH 1.68, 4.01, 7.00, and 10.00 and were not corrected for isotope effects. One-dimensional ^{1}H NMR spectra were recorded for AZR samples at 1 mM concentration in an H_2O/D_2O (9:1) solution at 13 different pH values between pH 0.85 and 7.00. Natural abundance ^{1}H-^{13}C-HSQC spectra with mixing times optimized for direct and long-range coupling constants (130 and 7 ms) were acquired using 20 mM AZR samples in a D_2O solution at seven different pH values in the 0.85−6.9 pH range. The decomposition of the compound prevented measurements at pH values higher than 7.0. Spectra were processed and analyzed using XWINNMR (Bruker, Rheinsteteen, Germany) and MESTRE-C.[39] The ^{1}H and ^{13}C chemical shifts were internally referenced using sodium 2,2-dimethyl-2-sila-pentane-5-sulfonate (DSS).

The ^{1}H NMR signals of Aztreonam were readily assigned on the basis of their chemical shift, multiplicity, and intensity. The ^{13}C resonances for carbons bound to protons were then straightforwardly identified from the cross-peaks observed in the ^{1}H-^{13}C-HSQC spectra optimized for direct couplings. Finally, the ^{13}C

chemical shifts of the remaining carbons were assigned from the ^{1}H-^{13}C-HSQC spectra optimized for long-range couplings. ^{1}H and ^{13}C chemical shifts are listed in Tables 1 and 2 and Table S1. Least-squares analysis (see Results) was performed using Microcal Origin v. 6.0.

MD/QM Calculations. MM Parametrization of AZR Tautomers. Initial coordinates for AZR were taken from the X-ray structure of its zwitterionic form cocrystallized with dimethylacetamide.[9] Then the various AZR configurations (**Z1**−**Z3**, **A1**−**A4**, **D1**) were generated by simple molecular modeling, and their geometries were relaxed at the HF/6-31+G* level of theory using the Onsager solvent continuum model ($\epsilon = 80.0$) as implemented in the Gaussian 03 suite of programs.[40] Subsequently, the atomic charges were computed for each configuration using the RESP fitting procedure and the gas-phase HF/6-31G* electrostatic potential. Most of the bond, angle, and dihedral parameters of AZR were available from the AMBER force field.[41] However, some structural data required to represent the equilibrium geometry of the β-lactam ring and the acyl-amino side chain were extracted from the HF/6-31+G* optimized structures. The van der Waals parameters were taken from the closest existing AMBER atom types using electronic similarity as a guide. In addition, some specific torsion parameters were included to properly reproduce the syn conformation of the *N*-SO_3^- group with respect to the acyl-amino side chain. These torsion parameters were adjusted against ab initio conformational energies and geometries obtained for a small model compound (3-formylamino-4-methyl-2-azetidine-1-sulfonate ion) at the MP2/6-31+G** level.

Molecular Dynamics Simulations. MD simulations in aqueous solution were carried out using the SANDER program included in the AMBER 8.0 suite of programs.[42] The time step was chosen to be 1.5 fs and the SHAKE algorithm was used to constrain all bonds involving hydrogen atoms. The solute was surrounded by a solvent box of TIP3P water molecules that extended 20 Å from the solute atoms. Periodic boundary conditions were applied to simulate a continuous system at constant pressure (1 atm) and temperature (300 K). To include the contributions of long-range interactions, the Particle−Mesh−Ewald (PME) method was used. To neutralize the negative charge of the anionic/dianionic forms, a uniform density with a total charge of +1/+2 was included in the PME calculations.[43] A cutoff of 10 Å was used to compute the vdW forces.

The solvent molecules were initially relaxed by means of energy minimizations and 60 ps of MD. Then the full systems were minimized followed by MD simulations. Trajectories were well equilibrated and were stable after 200 ps as evidenced by various properties (e.g., dimensions of the simulation box, energy components, etc.). Subsequently, 3 ns trajectories were computed, and the coordinates were saved for analysis at 10 ps intervals.

Sampled conformations from the MD trajectory were clustered using the NMRCLUST program.[44] This program uses the method of average linkage to define how clusters are constructed, followed by an application of a penalty function that simultaneously minimizes (1) the number of clusters and (2) the variation within each cluster. A minimum distance of 1.5 Å was used to select representative structures from each cluster. To characterize some networks of hydrogen bonds (water bridges), we assumed that a solvent H bond was present if both distance (i.e., O···O <3.5Å) and angular (i.e., O−H···O >120°) criteria were simultaneously satisfied. Geometrical averages were obtained using the CARNAL module of AMBER 8.0 and some other specific trajectory analysis software that was locally developed. Some figures were produced with the programs Molscript[45] and Raster3D.[46]

pK_a Calculations. Theoretically, pK_a values for a compound in aqueous solution can be formally calculated from the generalized thermodynamic cycle in Scheme 2. These pK_a calculations require reliable standard free energy calculations in gas-phase (ΔG_{gas}) as well as solvation energies (ΔG_{solv}) for the different species involved including the standard free energy of proton solvation, which is usually considered an additional parameter chosen to give the best match between calculated and experimental pK_a results.[18,47] We note that the accurate evaluation of the pK_a values of acid/base functional groups is a highly challenging issue in modern computational chemistry because a small error of 1.36 kcal/mol in the free energy of the corresponding deprotonation reaction results in a significant deviation of one pH unit in the pK_a.

Scheme 2

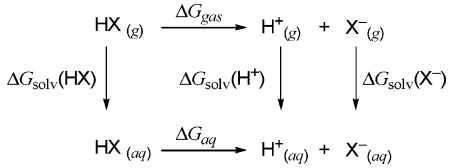

Here, the relative free energies in solution of the zwitterionic (**Z1**−**Z3**) and anionic (**A1**−**A4**) forms of AZR with respect to its dianionic configuration (**D1**) were computed as a function of pH by means of the following equation

$$\Delta G_{\mathrm{aq,i}} = G_{\mathrm{aq,i}} - G_{aq,\mathbf{D1}} - n_i G_{aq,\mathrm{H^+}} = \bar{G}^0_{\mathrm{aq,i}} - \bar{G}^0_{\mathrm{aq,D1}} - n_{\mathrm{i}} G^{+0}_{\mathrm{aq,H}} - n_{\mathrm{i}}(\ln 10 \cdot RT)\mathrm{pH} \quad (2)$$

where $G^{+0}_{\mathrm{aq,H}}$ represents the standard free energy of the proton and $n_{\mathrm{i}} = 2$ for $i =$ **Z1**−**Z3** and $n_{\mathrm{i}} = 1$ for $i =$ **A1**−**A4**.

The average standard free energies ($\bar{G}^0_{\mathrm{aq,i}}$) that appear in eq 2 were computed by means of the following computational protocol.

(1) For each AZR configuration, the coordinates of the solute and a solvent layer of 1000 water molecules centered on the C1@AZR atom were taken from 50 representative snapshots extracted every 60 ps along the corresponding MD trajectory.

(2) The selected sets of truncated snapshots were subject to energy minimization using the ONIOM method[48,49] implemented in the Gaussian03 suite of programs.[40] In the ONIOM calculations, the AZR molecule was described at the HF/3-21G* level of theory, whereas the surrounding water molecules were described by the TIP3P potential. In this way, we quantum mechanically relaxed the internal geometry of AZR, preserving its conformation in solution. We chose the ONIOM strategy because it represents a reasonable compromise between computational cost and accuracy.

(3) The free energy of the *j*th snapshot extracted from the MD trajectory of the *i*th configuration of AZR ($G_{\mathrm{i,j}}$), was estimated utilizing the following equation

$$G_{\mathrm{i,j}} = E^{\mathrm{elec}}_{\mathrm{i,j}} + E^{\mathrm{disp\ solute}}_{\mathrm{i,j}} + (\Delta G^{\mathrm{PB-SCRF}}_{\mathrm{i,j}} + \gamma A_{\mathrm{i,j}} + E^{\mathrm{disp\ solute-solvent}}_{\mathrm{i,j}}) \quad (3)$$

where $E^{\mathrm{elec}}_{\mathrm{i,j}}$ is the gas-phase electronic energy, and $E^{\mathrm{disp\ solute}}_{\mathrm{i,j}}$ is an empirical term that accounts for the solute intramolecular dispersion energy. The three terms in parentheses contribute to the solvation energy of the solute. The first one, $\Delta G^{\mathrm{PB-SCRF}}_{\mathrm{i,j}}$, is the electrostatic solvation energy, which is calculated using a DFT Hamiltonian coupled with a continuum model, whereas $\gamma A_{\mathrm{i,j}}$ and $E^{\mathrm{disp\ solute-solvent}}_{\mathrm{i,j}}$ are the cavitation and solute−solvent dispersion energies, respectively, which are computed using empirical formulas.

(3.1) The electronic energies ($E^{\mathrm{elec}}_{\mathrm{i,j}}$) in eq 3 were computed by means of single-point B3LYP/6-31+G** calculations[50] on the solute coordinates extracted from the ONIOM energy minimizations. Similarly, the electrostatic solvation energy ($\Delta G^{\mathrm{PB-SCRF}}_{\mathrm{i,j}}$) was taken into account by means of Poisson−Boltzmann self-consistent reaction field (PB−SCRF) calculations[51] at the B3LYP/6-31+G** level assuming a value of 80 for the dielectric constant of the surrounding continuum. Both the gas-phase and PB−SCRF calculations were carried out with the Jaguar program.[52]

(3.2) The dispersive contributions to eq 3 ($E^{\mathrm{disp\ solute}}_{\mathrm{i,j}}$ and $E^{\mathrm{disp\ solute-solvent}}_{\mathrm{i,j}}$) were computed using an empirical formula that has been introduced by Elstner et al.[53] to extend their approximate DFT method[54] to the description of dispersive interactions, which are normally neglected in both DFT and semi-empirical QM methods. The energy expression basically consists of a C_6/R^6 term,

which is appropriately damped for short R distances. The corresponding C_6 coefficients for each pair of interacting atoms are calculated from experimental atomic polarizabilities[55] so that the total E_{disp} energy can be consistently added to the energy expression of the DFT methods. In this work, we used the same parameters and combination rules as those described by Elstner et al.,[53] which in turn are based on previous work by Halgren.[56] The solute−solvent energies ($E_{i,j}^{disp\ solute-solvent}$) take into account the dispersive attractive interactions between the solute and the solvent layer consisting of 1000 water molecules.

(3.3) The cavity free energy of solvation ($\gamma A_{i,j}$) was determined by a molecular surface area dependent term[57,58] in which the surface tension proportionality constant γ was set to 69 kcal mol^{-1} Å^{-2}. The molecular surface area was determined using the molsurf program of the AMBER 8.0 suite, applying Bondi radii for the solute atoms and a water probe radius of 1.4 Å.

(4) Free energy contributions arising from changes in the degrees of freedom (translational, rotational, and vibrational) of the solute molecule were included by applying classical statistical thermodynamics. Because these calculations are highly computationally demanding, they were performed only for five snapshots extracted from the corresponding MD simulation of the AZR configurations. Analytical frequency calculations at the ONIOM(HF/3-21G:TIP3P) level of theory were carried out on the optimized geometry of the truncated snapshots (solute + 1000 water molecules). Subsequently, a submatrix of the full Hessian matrix, which was constructed by taking the matrix elements associated with the nuclear degrees of freedom from the solute, was diagonalized, and the resulting harmonic frequencies were used to compute thermal contributions (298 K 1 bar) to enthalpy ($H^{rot-tran-vib}$) and entropy ($S^{rot-tran-vib}$) within the ideal gas, rigid rotor, and harmonic oscillator approximations. Both enthalpy and entropy terms were corrected using the corresponding scaling factors proposed by Scott & Radom.[59]

(5) The mean value of the standard free energy ($\bar{G}^0_{aq,i}$) for the ith configuration of AZR was obtained by combining the free energy terms G_{ij} (eq 3) with the thermal contributions

$$\bar{G}^0_{aq,i} = \sum_{j=1}^{N} \frac{G_{i,j}}{N} + \sum_{k=1}^{M} \frac{H_{i,k}^{rot-trans-vib} - TS_{i,k}^{rot-trans-vib}}{M} \qquad (4)$$

where $N = 50$ and $M = 5$.

(6) The standard free energy of a proton (G^0_{aq,H^+}), which is required to compute the AZR relative free energies using eq 2, was estimated by combining the gas-phase free energy of a proton ($5/2\ RT - TS_{gas} = 1.48 - 7.76 = -6.28$ kcal/mol at 298 K and 1 atm) with its solvation free energy ($\Delta G_{solv}(H^+)$). Here, $\Delta G_{solv}(H^+)$ was treated as a parameter chosen to give the best match between calculated and experimental pK_a values for acetic acid (4.90), 2-amino-thiazol (5.36), thiazol (2.44), and methylamine (10.66). The calculated free energies in solution for these small molecules, which are directly relevant to the acid−base groups of AZR, were obtained by means of a computational protocol nearly identical to that employed for the individual AZR snapshots. The selected $\Delta G_{solv}(H^+)$ (−263.5 kcal/mol, in good agreement with the typical literature values[20]) gave a standard deviation of the computed pK_a values with respect to the experimental ones of ±0.4 pH unit.

NMR Calculations. Previous computational experience has shown that the level of theory of geometry optimization has only a moderate impact on the quality of ab initio NMR shifts.[60,61] In this work, the ^{13}C chemical shifts of AZR were calculated with the ONIOM(HF/3-21G*//AMBER) optimized geometries and by employing the gauge-invariant atomic orbital (GIAO) method.[62] Thus, for the **Z1**, **A1**, **A2**, and **D1** tautomeric forms, we carried out 50 GIAO-B3LYP calculations with a 6-31+G** basis set. In these GIAO-B3LYP/6-31+G** calculations, the electrostatic effects of the aqueous solvent was taken into account by means of the polarizable continuum model (PCM) method.[63] The resulting ^{13}C NMR chemical shifts were averaged and referenced to $(CH_4)_4Si$ (calculated absolute shift, i.e., $\sigma(C) = 194.9$ at the GIAO-B3LYP/6-31+G**//HF/3-21G* level). All of the GIAO-B3LYP PCM calculations were performed with the Gaussian03 program.[40]

Acknowledgment. We thank Dr D. V. Laurents for help with English usage. This research was supported by the FICyT (Asturias, Spain) via grant PB02-045, the Ramon y Cajal program of the MEC (Spain), and the Junta de Castilla y León (Spain) via grant LE 09/04.

Supporting Information Available: 1D ^{1}H-NMR spectrum of AZR, titration curves for carbons 6−12, selected regions of the 7 ms ^{1}H-^{13}C-HSQC spectra, sum of gas phase solvation energies for the 50 snapshots, the theoretical titration curves, and experimental ^{13}C chemical shifts. This material is available free of charge via the Internet at http://pubs.acs.org.

References

(1) Livingstone, D. J. Theoretical property predictions. *Curr. Top. Med. Chem.* **2003**, *3*, 1171−1192.
(2) Martin, Y. C. A bioavailability score. *J. Med. Chem.* **2005**, *48*, 3164−3170.
(3) Szakacs, Z.; Béni, S.; Varga, Z.; Örfi, L.; Kéri, G. et al. Acid−base profiling of imatinib (gleevec) and its fragments. *J. Med. Chem.* **2005**, *48*, 249−255.
(4) Ulander, J.; Broo, A. Use of empirical correction terms in calculating ionization constants. *Int. J. Quantum Chem.* **2005**, *105*, 866−874.
(5) Sykes, R. B.; Bonner, D. P.; Bush, K.; Georgopapadakou, N. H. Aztreonam (sq 26, 776), a synthetic monobactam specifically active againts aerobic gram-negative bacteria. *Antimicrob. Agents Chemother.* **1982**, *21*, 85−92.
(6) Florey, K. Aztreonam. *Analytical Profiles of Drug Substances*; Academic Press: New York, 1988; pp 1−39.
(7) *Pubchem*: A molecular libraries road map initiative; National Center for Biotechnology Information, Bethesda, MD, 2005.
(8) Irwin, J. R.; Shoichet, B. K. Zinc − a free database of commercially available compounds for virtual screening. *J. Chem. Inf. Model.* **2005**, *45*, 177−182.
(9) Sowek, J. A.; Singer, S. B.; Ohringer, S.; Malley, M. F.; Dougherty, T. J.; et al. Substitution of lysine at position 104 or 240 of TEM-1PTZ18r β-lactamase enhances the effect of serine-164 substitution on hydrolysis or affinity for cephalosporins and the monobactam aztreonam. *Biochemistry* **1991**, *30*, 3179−3188.
(10) Oefner, C.; D′Arcy, A.; Daly, J. J.; Gubernator, K.; Charnas, R. L.; et al. Refined crystal structure of β-lactamase from *Citrobacter freundii* indicates a mechanism for β-lactam hydrolysis. *Nature* **1990**, *343*, 284−288.
(11) Hilal, S. H.; Karickhoff, S. W.; Carreira, L. A. Prediction of chemical reactivity parameters and physical properties of organic compounds from molecular structure using Sparc; U. S. Environmental Protection Agency: Athens, GA, 2003.
(12) Sparc online calculator. http://ibmlc2.chem.uga.edu/sparc/, 2003.
(13) Yoshimura, F.; Nikaido, H. Diffusion of β-lactam antibiotics through the porin channels of *Escherichia coli* K-12. *Antimicrob. Agents Chemother.* **1985**, *27*, 84−92.
(14) Satake, S.; E., Y.; Nakae, T. Diffusion of β-lactam antibiotics through liposome membranes reconstituted from purified porins of the outer membrane of *Pseudomonas aeruginosa*. *Antimicrob. Agents Chemother.* **1990**, *34*, 685−690.
(15) Fisher, J. F.; Meroueh, S. O.; Mobashery, S. Bacterial resistance to β-lactam antibiotics: Compelling opportunism, compelling opportunity. *Chem. Rev.* **2005**, *105*, 395−424.
(16) Kallies, B.; Mitzner, R. pK_a values of amines in water from quantum mechanical calculations using a polarized dielectric continuum representation of the solvent. *J. Phys. Chem. B* **1997**, *101*, 2959−2967.
(17) Topol, I. A.; Tawa, G. J.; Burt, S. K.; Rashin, A. A. Calculation of absolute and relative acidities of substituted imidazoles in aqueous solvent. *J. Phys. Chem. A* **1997**, *101*, 10075−10081.
(18) Jang, Y. H.; Sowers, L. C.; Çagin, T.; Goddard, W. A. I. First principles calculation of pK_a values for 5-substituted uracils. *J. Phys. Chem. A* **2001**, *105*, 274−280.
(19) Liptak, M. D.; Shields, G. C. Accurate pK_a calculations for carboxylic acids using complete basis set and Gaussian-n models combined with CPCM continuum solvation methods. *J. Am. Chem. Soc.* **2001**, *123*, 7314−1719.
(20) Liptak, M. D.; Gross, K. C.; Seybold, P. G.; Feldgus, S.; Shields, G. C. Absolute pK_a determinations for substituted phenols. *J. Am. Chem. Soc.* **2002**, *124*, 6421−6427.
(21) Lopez, X.; Schaefer, M.; Dejaegere, A.; Karplus, M. Theoretical evaluation of pK_a in phosphoranes: Implications for phosphate ester hydrolysis. *J. Am. Chem. Soc.* **2002**, *124*, 5010−5018.

(22) Noyes Rogstad, K.; H., J. Y.; Sowers, L. C.; Goddard, W. A., III First principles calculations of the pK_a values and tautomers of isoguanine and xanthine. *Chem. Res. Toxicol.* **2003**, *16*, 1455−1462.
(23) Jang, Y. H.; Goddard, W. A., I.; Noyes, K. T.; Sowers, L. C.; Hwang, S. et al. pK_a values of guanine in water: Density functional theory calculations combined with Poisson−Boltzmann continuum-solvation model. *J. Phys. Chem. B* **2003**, *107*, 347−357.
(24) Fu, Y.; Liu, L.; Li, R.-Q.; Liu, R.; Guo, Q.-X. First-principle predictions of absolute pK_a's of organic acids in dimethyl sulfoxide solution. *J. Am. Chem. Soc.* **2004**, *126*, 814−822.
(25) Yang, P.; Murthy, P. P. N.; Brown, R. E. Synergy of intramolecular hydrogen-bonding network in myo-inositol 2-monophosphate: Theoretical investigations into the electronic structure, proton transfer, and pK_a. *J. Am. Chem. Soc.* **2005**, *127*, 15848−15861.
(26) Kelly, C. P.; Cramer, C. J.; Truhlar, D. G. Adding explicit solvent molecules to continuum solvent calculations for the calculation of aqueous acid dissociation constants. *J. Phys. Chem. A* **2006**, *110*, 2493−2499.
(27) Jensen, J. H.; Li, H.; Robertson, A. D.; Molina, P. A. Prediction and rationalization of protein pK_a values using QM and QM/MM methods. *J. Phys. Chem. A* **2005**, *109*, 6634−6643.
(28) Pérez-Cañadillas, M.; Campos-Olivas, R.; Lacadena, J.; del-Pozo, A. M.; Gavilanes, J. G.; et al. Characterization of pK_a values and titration shifts in the cytotoxic ribonuclease α-sarcin by NMR. Relationships between electrostatic interactions structure and catalytic function. *Biochemistry* **1998**, *37*, 15865−15876.
(29) Forman-Kay, J. D.; Clore, G. M.; Gronenborn, A. M. Relationship between electrostatics and redox function in human thioredoxin: Characterization of pH titration shifts using two-dimensional homo- and heteronuclear NMR. *Biochemistry* **1992**, *31*, 3442−3452.
(30) Primrose, W. U. *NMR of Macromolecules. A Practical Approach*; Oxford University Press: Oxford, 1993; pp 22−23.
(31) Peck, C. C.; Benet, L. Z. General method for determining macrodissociation constants of polyprotic, amphoteric compounds from solubility measurements. *J. Pharm. Sci.* **1978**, *67*, 12−16.
(32) Hilal, S. H.; Karickhoff, S. W.; Carreira, L. A. Verification and validation of the SPARC model; U.S. Environmental Protection Agency: Athens, GA, 2003.
(33) Díaz, N.; Suárez, D.; Sordo, T. L. Molecular dynamics simulations of class C β-lactamase from *Citrobacter freundii*: Insights into the base catalyst for acylation. *Biochemistry* **2006**, *45*, 439−451.
(34) Riccardi, D.; Schaefer, P.; Cui, Q. pK_a calculations in solution and proteins with QM/MM free energy perturbation simulations: A quantitative test of QM/MM protocols. *J. Phys. Chem. B* **2005**, *109*, 17715−17733.
(35) Ramalho, T. C.; da Cunha, E. F. F.; de Alencastro, R. B. Solvent effects on ^{13}C and ^{15}N shielding tensors of nitroimidazoles in the condensed phase: A sequential molecular dynamics/quantum mechanics study. *J. Phys. Condens. Matter* **2004**, *16*, 6159−6170.
(36) Cappelli, C.; Mennucci, B.; Monti, S. Environmental effects on the spectroscopic properties of gallic acid: A combined classical and quantum mechanical study. *J. Phys. Chem. A* **2005**, *109*, 1933−1943.
(37) Kollman, P. A.; Massova, I.; Reyes, C.; Kuhn, B.; Huo, S.; et al. Calculating structures and free energies of complex molecules: Combining molecular mechanics and continuum models. *Acc. Chem. Res.* **2000**, *33*, 889−897.
(38) Raha, K.; Merz, K. M. Large-scale validation of a quantum mechanics based scoring function: Predicting the binding affinity and the binding mode of a diverse set of protein−ligand complexes. *J. Med. Chem.* **2005**, *48*, 4558−4575.
(39) Cobas, J. C.; Sardina, F. J. Nuclear magnetic resonance data processing. Mestre-C: A software package for desktop computers. *Concepts Magn. Reson., Part A* **2003**, *19A*, 80−96.
(40) Frisch, M. J.; Trucks, G. W.; Schlegel, H. B.; Scuseria, G. E.; Robb, M. A.; Cheeseman, J. R.; Montgomery, J. A., Jr.; Vreven, T.; Kudin, K. N.; Burant, J. C.; Millam, J. M.; Iyengar, S. S.; Tomasi, J.; Barone, V.; Mennucci, B.; Cossi, M.; Scalmani, G.; Rega, N.; Petersson, G. A.; Nakatsuji, H.; Hada, M.; Ehara, M.; Toyota, K.; Fukuda, R.; Hasegawa, J.; Ishida, M.; Nakajima, T.; Honda, Y.; Kitao, O.; Nakai, H.; Klene, M.; Li, X.; Knox, J. E.; Hratchian, H. P.; Cross, J. B.; Bakken, V.; Adamo, C.; Jaramillo, J.; Gomperts, R.; Stratmann, R. E.; Yazyev, O.; Austin, A. J.; Cammi, R.; Pomelli, C.; Ochterski, J. W.; Ayala, P. Y.; Morokuma, K.; Voth, G. A.; Salvador, P.; Dannenberg, J. J.; Zakrzewski, V. G.; Dapprich, S.; Daniels, A. D.; Strain, M. C.; Farkas, O.; Malick, D. K.; Rabuck, A. D.; Raghavachari, K.; Foresman, J. B.; Ortiz, J. V.; Cui, Q.; Baboul, A. G.; Clifford, S.; Cioslowski, J.; Stefanov, B. B.; Liu, G.; Liashenko, A.; Piskorz, P.; Komaromi, I.; Martin, R. L.; Fox, D. J.; Keith, T.; Al-Laham, M. A.; Peng, C. Y.; Nanayakkara, A.; Challacombe, M.; Gill, P. M. W.; Johnson, B.; Chen, W.; Wong, M. W.; Gonzalez, C.; Pople, J. A. *Gaussian 03*, revision C.02; Gaussian, Inc.: Wallingford, CT, 2004.
(41) Cornell, W. D.; Cieplak, P.; Bayly, C. I.; Gould, I. R.; Merz, K. M., Jr.; et al. A second generation force field for the simulation of proteins, nucleic acids, and organic molecules. *J. Am. Chem. Soc.* **1995**, *117*, 5179−5197.
(42) Case, D. A.; Darden, T. A.; Cheatham, T. E. I.; Simmerling, C. L.; Wang, J.; et al. *AMBER 8*, edition 8.0; University of California: San Francisco, CA, 2004.
(43) Sagui, C.; Darden, T. A. Molecular dynamic simulations of biomolecules long-range electrostatic effects. *Annu. Rev. Biophys. Biomol. Struct.* **1999**, *28*, 155−179.
(44) Kelley, L. A.; Gardner, S. P.; Sutcliffe, M. J. An automated approach for clustering an ensemble of NMR-derived protein structures into conformationally related subfamilies. *Protein Eng.* **1996**, *9*, 1063−1065.
(45) Kraulis, P. J. Molscript: A program to produce both detailed and schematic plots of protein structures. *J. Appl. Crystallogr.* **1991**, *24*, 946−950.
(46) Merritt, E. A.; Bacon, D. J. Raster3d: Photorealistic molecular graphics. *Methods Enzymol.* **1997**, *277*, 505−524.
(47) Schmidt am Bush, M.; Knapp, E. W. Accurate pK_a determination for a heterogeneous group of organic molecules. *ChemPhysChem* **2004**, *5*, 1513−1522.
(48) Dapprich, S.; Komaromi, I.; Byun, K.; Morokuma, K.; Frisch, M. J. A new ONIOM implementation in *Gaussian98*. *J. Mol. Struct. (THEOCHEM)* **1999**, *461*, 1−21.
(49) Vreven, T.; Morokuma, K.; Farkas, O.; Schlegel, H. B.; Frisch, M. J. Geometry optimization with QM/MM, ONIOM, and other combined methods. I. Microiterations and constraints. *J. Comput. Chem.* **2003**, *24*, 760−769.
(50) Becke, A. D. Exchange-correlation approximation in density-functional theory. *Modern Electronic Structure Theory Part II*; World Scientific: Singapore, 1995.
(51) Tannor, D. J.; Marten, B.; Murphy, R.; Friesner, R. A.; Sitkoff, D.; et al. Accurate first principles calculation of molecular charge distributions and solvation energies from ab initio quantum mechanics and continuum dielectric theory. *J. Am. Chem. Soc.* **1994**, *116*, 11875−11882.
(52) *Jaguar*, edition 5.5; Schrödinger, L.LC.: Portland, OR, 2003.
(53) Elstner, M.; Hobza, P.; Frauenheim, T.; Suhai, S.; Kaxiras, E. Hydrogen bonding and stacking interactions of nucleic acid base pairs: A density-functional-theory based treatment. *J. Chem. Phys.* **2001**, *114*, 5149−5154.
(54) Elstner, M.; Porezag, D.; Jungnickel, G.; Elsner, J.; Haugk, M.; et al. Self-consistent-charge density-functional tight-binding method for simulations of complex materials properties. *Phys. Rev. B: Condens. Matter* **1998**, *58*, 7260−7268.
(55) Miller, K. J. Additivity methods in molecular polarizability. *J. Am. Chem. Soc.* **1990**, *112*, 8533−8542.
(56) Halgren, T. A. Representation of van der Waals (vdW) interactions in molecular mechanics force fields: Potential form, combination rules, and vdW parameters. *J. Am. Chem. Soc.* **1992**, *114*, 7827−7843.
(57) Gohlke, H.; Case, D. A. Converging free energy estimates: MM-PB(GB)SA studies on the protein -protein complex Ras−Raf. *J. Comput. Chem.* **2003**, *25*, 238−250.
(58) Ashbaugh, H. S.; Kaler, E. W.; Paulaitis, M. E. A "universal" surface area correlation for molecular hydrophobic phenomena. *J. Am. Chem. Soc.* **1999**, *121*, 9243−9244.
(59) Scott, A. P.; Radom, L. Harmonic vibrational frequencies: An evaluation of Hartree−Fock, Møller−Plesset, Quadratic Configuration Interaction, Density Functional Theory, and Semiempirical scale factors. *J. Phys. Chem.* **1996**, *100*, 16502−16513.
(60) Rablen, P. R.; Pearlman, S. A.; Finkbiner, J. A comparison of density functional methods for the estimation of proton chemical shifts with chemical accuracy. *J. Phys. Chem. A* **1999**, *105*, 7357−7363.
(61) Giesen, D. J.; Zumbulyadis, N. A hybrid quantum mechanical and empirical model for the prediction of isotropic 13c shielding constants of organic molecules. *Phys. Chem. Chem. Phys.* **2002**, *4*, 5498−5507.
(62) Wolinski, K.; Hinton, J. F.; Pulay, P. Efficient implementation of the gauge-independent atomic orbital method for NMR chemical shift calculations. *J. Am. Chem. Soc.* **1990**, *112*, 8251−8260.
(63) Cammi, R.; Mennucci, B.; Tomasi, J. Nuclear magnetic shieldings in solution: Gauge invariant atomic orbital calculation using the polarizable continuum model. *J. Chem. Phys.* **1999**, *110*, 7627−7638.

JM060096T